Chinese Chemical Letters 35 (2024) 108340

Contents lists available at ScienceDirect

Chinese Chemical Letters

journal homepage: www.elsevier.com/locate/cclet

How ligand coordination and superatomic-states accommodate the structure and property of a metal cluster: $Cu_4(dppy)_4Cl_2$ *vs.* $Cu_{21}(dppy)_{10}$ with altered photoluminescence

Haiming Wu[a,1], Gaya N. Andrew[a,1], Rajini Anumula[a], Zhixun Luo[a,b,*]

[a] *Beijing National Laboratory for Molecular Sciences (BNLMS), State Key Laboratory for Structural Chemistry of Unstable and Stable Species, Institute of Chemistry, Chinese Academy of Sciences, Beijing 100190, China*
[b] *School of Chemistry, University of Chinese Academy of Sciences, Beijing 100049, China*

ARTICLE INFO

Article history:
Received 31 December 2022
Revised 1 March 2023
Accepted 13 March 2023
Available online 15 March 2023

Keywords:
Copper nanocluster
Yellow emission
Dual emission
Superatomic states
Ligand dppy

ABSTRACT

We have synthesized two copper nanoclusters (NCs) with a protection of the same ligand diphenylphosphino-2-pyridine ($C_{17}H_{14}NP$, dppy for short), formulated as $Cu_4(dppy)_4Cl_2$ and $Cu_{21}(dppy)_{10}$, respectively. The former one bears a distorted tetrahedron Cu_4 core with its six edges fully protected by chlorine and dppy ligands, while the latter presents a symmetric Cu_{21} core on which ten dppy molecules function as monolayer protection *via* well-organized monodentate or bidentate coordination. Interestingly, the $Cu_4(dppy)_4Cl_2$ cluster exhibits a strong yellow emission at ~577 nm, while $Cu_{21}(dppy)_{10}$ displays dual emissions in purple (~368 nm) and green (~516 nm) regions respectively. In combination with TD-DFT calculations, we demonstrate the origin of altered emissions and unique stability of the two copper nanoclusters pertaining to the ligand coordination and metallic superatomic states.

Ligand-protected metal nanoclusters (NCs for short) allow for tuneable charge distribution and energy transfer between the metallic core and organic ligands, giving rise to a diversity of structures, compositions and crystalline forms [1–4]. Due to the unique electron configuration $(n\text{-}1)d^{10}ns^1$ [5], coinage metal NCs have shown their advantages of facile synthesis and distinctive optical, electrical and chemical properties with promising applications in chemo-sensing, bio-labelling and catalysis [6–9]. The Cu NCs are of special interest because they usually exhibit earth-abundant, cost-efficient and luminesce properties due to weak spin-orbit coupling interaction and high reorganization energy under photoexcitation [10–12]. However, the single crystal synthesis of Cu NCs is challenging due to the lower M^I/M^0 half-cell potential of Cu (0.52 V) compared with that of Ag (0.80 V) and Au (1.68 V) [13–15]. Difficult as was the work, significant advances have been made to synthesize the ligand-protected Cu NCs, such as those of thiolate [16,17], phosphine [18], selenate [19], alkynyl [20] and halogen ligands [21–23], shedding light on the powerful ligand engineering which causes a diversity of cluster structures.

Along with the significant advances in synthesizing atomically precise metal NCs, it is recognized that superatomic electron configuration profits to thermal stability of metal NCs [24,25]; also, both ligand accommodation and superatomic states are sensitive to cluster sizes [26–29]. Some stable metal NCs are rationalized with a magic number of valence electrons simply by considering that the highly electrophilic ligands capture electrons of the metallic core. This has been applied for 2e-superatomic $[Cu_{13}(S_2CN^nBu_2)_6(acetylide)_4]^+$ [30], 8e-superatomic $[Ag_{21}\{S_2P(OiPr)_2\}_{12}]^+$ [31], 18e-superatomic $Au_{44}(DMBT)_{26}$ [32], 20e-superatomic $Pd_{55}(PiPr_3)_{12}(CO)_{20}$ [33], 34e-superatomic $[Ag_{78}(^i PrPhS)_{30}(dppm)_{10}Cl_{10}]^{4+}$ [34], 58e-superatomic $[Au_{69}(PR_3)_{20}Cl_{12}]^-$ and $Au_{102}(p\text{-}MBA)_{44}$ NCs [35,36]. Apart from the successful synthesis of diverse metal NCs, ongoing efforts have been devoted to understanding how ligand coordination and metal superatomic-states accommodate the structure and property of a metal cluster, thus beneficial to rational design of cluster-based functional materials.

A versatile ligand, diphenylphosphino-2-pyridine (dppy for short), has been widely applied in the synthesis of luminescent metal NCs [37–39], and the flexibility of its bidentate or monodentate coordination enables for tuneable accommodation [40–43]. Here we report a comparative study on the contributions of both superatomic stability and ligand coordination to the copper NCs by utilizing the dppy as ligand. With reduction of $[Cu(OAc)_2]$

* Corresponding author at: Beijing National Laboratory for Molecular Sciences (BNLMS), State Key Laboratory for Structural Chemistry of Unstable and Stable Species, Institute of Chemistry, Chinese Academy of Sciences, Beijing 100190, China.
E-mail address: zxluo@iccas.ac.cn (Z. Luo).
[1] These authors contributed equally to this work.

https://doi.org/10.1016/j.cclet.2023.108340
1001-8417/

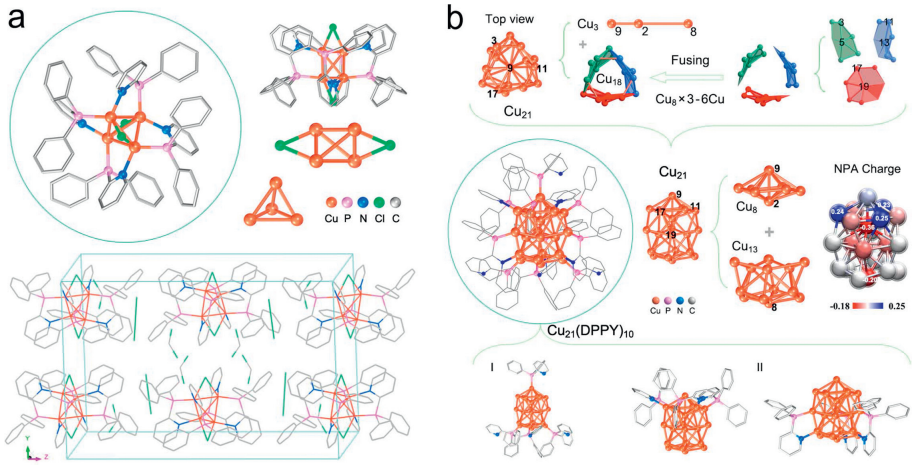

Fig. 1. Single-crystal structures of (a) $Cu_4(dppy)_4Cl_2$, with a CH_2Cl_2 and a Cl_3 involved and (b) $Cu_{21}(dppy)_{10}$. The insets include the natural population analysis (NPA) of charge distribution of Cu_{21} nanocluster. Cu in orange, P pink, N blue, Cl green, and C grey. For clarity, H atoms are omitted. Capped sticks and ball-stick styles (instead of thermal ellipsoids) are displayed for the two kinds of Cu clusters.

in the presence of $NaBH_4$, we have synthesized the single-crystals of two luminescent clusters, $Cu_4(dppy)_4Cl_2$ and $Cu_{21}(dppy)_{10}$ NCs. Amongst them, the $Cu_{21}(dppy)_{10}$ cluster shows a superatomic metallic core but allow for well-organized monodentate and bidentate coordination of the dppy ligands. Interestingly, the Cu_{21} NCs exhibit dual emissions in purple and green regions; in comparison, the $Cu_4(dppy)_4Cl_2$ cluster has a tetrahedron Cu_4 core *via* full protection by bridged sulfur of the monodentate dppy ligands, giving rise to a broad band of yellow emission at ~577 nm.

Fig. 1a displays the single-crystal structure of the $Cu_4(dppy)_4Cl_2$ NCs (Figs. S1 and S2, Table S1 in Supporting information). Single-crystal parsing results at 110 K show that the $Cu_4(dppy)_4Cl_2$ NCs are crystallized in a monoclinic crystal system with a space group of I2/a. The single-crystal composition is determined to be $Cu_4P_4N_4C_{70}H_{60}Cl_9$, with two additional non-coordination moieties CH_2Cl_2 and Cl_3 being involved in the single crystals [44–50]. Interestingly, the metallic core displays a slightly distorted tetrahedron Cu_4 of which each Cu atom is coordinated with its adjacent three Cu atoms with average Cu-Cu distance at 2.821 Å (2.651–2.956 Å). Meanwhile, four dppy ligands form bidentate coordination on four edges of the tetrahedron Cu_4 core of which the other two edges are linked with chlorine bridges, giving rise to full protection of the six edges of the Cu_4 core. Also, each Cu atom binds to its adjacent three Cu atoms, and is simultaneously coordinated with N, P and Cl atoms. Natural population analysis (NPA) shows that the charge distribution on each Cu and Cl atom is 0.20e and −0.60e respectively (Fig. S15 and Table S2 in Supporting information), indicative of electron attraction of chlorine rendering a 2e-superatomic Cu_4 core (4e - 0.6e × 2 - 0.2e × 4 = 2e). The saturated hexa-coordinate of copper, and the well-organized charge transfer interactions account for the prominent stability of such a 2e-superatomic copper cluster [51–54].

We have synthesized a larger copper cluster $Cu_{21}(dppy)_{10}$ with the same ligand and similar procedure, but find there is a different case of the structure and coordination modes. Fig. 1b dissects the single crystal structure of the as-prepared Cu_{21} NCs (Figs. S3–S5 and Table S1 in Supporting information). The single-crystal parsing reveals that the $Cu_{21}(dppy)_{10}$ is crystallized in a trigonal space group with a precise composition of $Cu_{21}C_{170}H_{140}N_{10}P_{10}$. The *quasi* C_3-symmetric Cu_{21} core can be viewed as the connection of a gyroscopic-like Cu_8 and a bottom bowl-like Cu_{13} along the line through the atoms of Cu9, Cu2 and Cu8. In the Cu_{13} moiety, the Cu-Cu average distance is 2.652 Å (2.477–2.994 Å), which is almost equal to the Cu-Cu bond length (averaged at 2.651 Å) in the Cu_8 moiety (Fig. S16 and Table S3 in Supporting information), but smaller than the average Cu-Cu bond length in $Cu_4(dppy)_4Cl_2$. The varied Cu-Cu bond lengths are also consistent with the previously reported Cu NCs [55–58], due to flexible Cu coordination. Different from $Cu_4(dppy)_4Cl_2$, the Cu_{21} core is stabilized by ten dppy ligands which form two types of coordination bonds. Four of the ten dppy ligands bind to four Cu atoms through Cu-P bonds, while the other six ligands bind to twelve Cu atoms by six Cu-P bonds and six Cu-N bonds, and additional five Cu atoms do not link to the ligand (including the central atom Cu8). This is different from the other Cu NCs protected by the dppy ligands [59]. The average Cu-P bond length in $Cu_{21}(dppy)_{10}$ is similar to that of the Cu(I) phosphine complex [60] and the $[Cu_{25}H_{22}(PPh_3)_{12}]Cl$ cluster [61]. The calculated NPA charge distribution (based on the single crystal structure) reveals that there are different types of Cu atoms involved in the $Cu_{21}(dppy)_{10}$. Specifically, the body-centred Cu atom (Cu2) and bottom-centred Cu atom (Cu8) are largely negative (−0.36 and −0.20|e|); the three vertex atoms of the gyroscopic-like Cu_8 moiety (*i.e.*, Cu1, Cu10, Cu19) are positively charged (0.24, 0.23 and 0.25|e|); the three face-centred (Cu5, Cu13, Cu19) and three vertex Cu atoms (Cu3, Cu11, Cu17) of the three heptagons are slightly negative, while the other Cu atoms are slightly positive or close to zero. Note that, the total NPA charge of the capping gyroscopic-like Cu_8 region is 0.29|e|, while the total NPA of bottom bowl-like Cu_{13} is −0.19|e|. Although a diversity of the NPA charge distribution on the coper atoms, the total NPA charge on the Cu_{21} core is close to zero (Fig. S17 and Tables S4–S6 in Supporting information), which is in sharp contrast to that of the Cu_4 core at 0.80|e|, showing a different mechanism of stability.

Fig. 2 presents the typical mass spectra of the two copper NCs, collected in a positive mode *via* an electrospray ionization mass spectrometer (ESI-MS). Notably, there are two prominent peaks for the $Cu_4(dppy)_4Cl_2$ NCs at *m/z* 1379.01 and 1422.96, corresponding to $[Cu_4(dppy)_4Cl_2+H]^+$ and $[Cu_4(dppy)_4Cl_2+2Na]^+$. Besides, the peak at *m/z* 1466.93 could be assigned to $[Cu_4(dppy)_4Cl_2{\cdot}CH_2Cl_2+5H]^+$. The absence of other strong abundance peaks suggests high chemical purity and stability of the $Cu_4(dppy)_4Cl_2$ NCs. Note that the experimental isotopic pattern and simulated mass distribution match well with each other (insets in Fig. 2a). Similarly, Fig. 2b shows the ESI-MS spectrum of Cu_{21} NCs, where a small peak at *m/z* 1991.76 is assigned to $[Cu_{21}(DPPY)_{10}+17H]^{2+}$, of which the isotopic patterns match with the simulated mass distribution (insets in Fig. 2b). A few fragment peaks are also seen at *m/z* 1707.64, 1838.28 and 1903.24, corre-

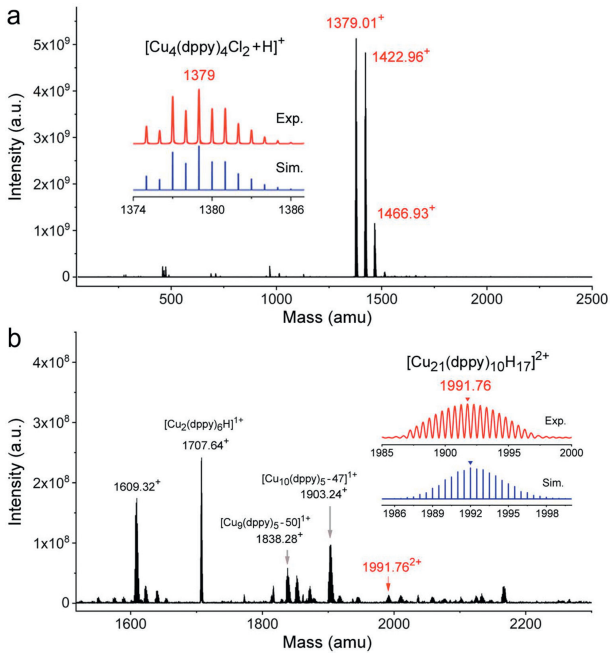

Fig. 2. ESI-MS of (a) $Cu_4(dppy)_4Cl_2$ and (b) $Cu_{21}(dppy)_{10}$ NCs in the positive ion mode, respectively. Insets display the experimental spectrum in a comparison with the simulated isotopic patterns.

sponding to dissociation and hydrogenation of the copper core as well as the loss of a few dppy ligands. This also agrees with the phosphine-protected Ag clusters due to weak bonding interactions [62].

We have studied the absorption and photoluminescence properties of the two copper NCs. Fig. 3a shows the absorption spectrum of $Cu_4(dppy)_4Cl_2$ NCs in DCM, where a characteristic peak at 260 nm and a weak broad band at 472 nm are observed. For this small cluster, we have conducted TD-DFT calculations and check out all the likely electronic excitation transitions at the optimized S_0 minima of $Cu_4(dppy)_4Cl_2$ (Table S7 in Supporting information). As a result, the 260 nm peak is primarily caused by some *quasi*-degenerate electronic transitions (*e.g.*, HOMO → LUMO+30/31). Considering that the HOMO is mainly located on the Cu_4 metal core, while the LUMO+30/31 are contributed by the ligands, the electronic transition at ~260 nm corresponds to metal-to-ligand charge transfer (MLCT) transition. This is consistent with the previous reported study [63]. Besides, the TD-DFT calculations also find electronic transitions at 436, 518 and 546 nm, associated with the frontier molecular orbitals, which interprets the experimental observation of a broad weak band at 400–600 nm. Fig. 3b shows the photoluminescence spectrum of the $Cu_4(dppy)_4Cl_2$ NCs in DCM, where a remarkable yellow emission band at 577 nm is displayed. The quantum yield of the copper NC at room temperature is estimated to be ~1.83%. This is consistent with the previously reported halogen-protected copper NCs which also exhibit yellow emission at ~600 nm [64,65]. Time-resolved decay measurements were also carried out for the Cu_4 NC in DCM (Fig. 3c), where the yellow emission is associated with a relatively long lifetime of 121.87 ns. Furthermore, we measured the emission spectra of the $Cu_4(dppy)_4Cl_2$ NCs in altered low temperatures (Fig. 3d), and found that the luminescence shows enhanced intensity with decreasing temperature from 298 K to 150 K, while minor attenuation of intensity from 125 K to 78 K. Notably, the emission at 78 K shows a much longer lifetime up to microsecond (with fitted values at 46.03 μs and 95.50 μs). This is different from the monotonic increase tendency of low temperature phosphorus emission of small organic molecules. It is inferred that the dramatic changes of emission intensity and lifetime of such copper NCs could be associated with both electronic transitions between singlet and triplet states, as well as vibrational relaxation of the structure.

Similarly, Fig. 3e shows a typical UV–vis absorption spectrum of the $Cu_{21}(dppy)_{10}$ NCs in DCM, where a characteristic peak appears at 258 nm. This is consistent with the excitation spectrum (Fig. S12 in Supporting information), and similar to the absorption spectrum of the aforementioned $Cu_4(dppy)_4Cl_2$ NCs because their frontier orbitals are mainly contributed by copper. Further, we examined the luminescent property (Fig. 3f), where dual emissions at two bands are observed, namely, the purple at 368 nm and green at 516 nm regions. By changing the excitation wavelength to 290 nm (Fig. S13 in Supporting information), the two-band emissions retain and display minor redshifts. Notably, the green emission at 516 nm is much stronger than the purple emission, contributed by the dppy ligand which has an emission at 500 nm (Fig. S11 in Supporting information). It is worth mentioning that the FWHM of the 516 nm emission of $Cu_{21}(dppy)_{10}$ NCs is relatively narrower than that of the $Cu_4(dppy)_4Cl_2$ NCs (143 nm *vs.* 160 nm). The fluorescence variation of the two copper NCs could be related to the symmetry of the protective ligands and the different copper core. Time-resolved fluorescence decay measurements were also carried out for the $Cu_{21}(dppy)_{10}$ NCs. As shown in Figs. 3g and h, the purple and green emissions are associated with short lifetime, with fitted values for purple emission at 3.37 ns and green emission at 0.08 ns and 2.81 ns. This short lifetime of copper NCs is consistent with previous studies [66]. For the purple and green emissions, we have also measured the quantum yield in DCM but found very small values (*ca.* 0.2% and 2%, respectively).

To elucidate the origin of the stability and optical properties of the two copper NCs, by DFT-calculations we have performed an analysis on the canonical molecular orbitals (CMOs), Kohn-Sham molecular orbital energy levels, total and partial density of states (DOSs) of both $Cu_4(dppy)_4Cl_2$ and $Cu_{21}(dppy)_{10}$ NCs (Fig. 4). It is noteworthy that the Cu atoms significantly contribute to the orbitals ranging from HOMO to HOMO-19 (>50%) at optimized S_0 minima of $Cu_4(dppy)_4Cl_2$, with a large HOMO-LUMO energy gap up to 2.34 eV, which is consistent with the DOS patterns shown in Fig. 4a (Table S8 in Supporting information). Notably, the HOMO of $Cu_4(dppy)_4Cl_2$ exhibits superatomic S orbital pattern, shedding light on the 2e-superatomic feature. In comparison, the CMOs of $Cu_{21}(dppy)_{10}$ reflect more superatomic states, as shown in Fig. 4b (Figs. S18–S21 and Table S9 in Supporting information), where the superatomic 1S, 1P and 1D orbitals can be recognized, indicative of 18e-superatomic stability. As a comparison, we have also conducted a calculation on the cationic $[Cu_{21}(dppy)_{10}]^+$ and find similar superatomic orbitals (1S|1P|1D||) along with an enlarged HOMO-LUMO gap. The inherent superatomic states in such metal NCs, embodied by partly itinerant (/delocalized) electrons, enable to balance the nuclear-electron interactions and thus optimal accommodation on the metal-metal bonding and metal-ligand interactions [67,68].

Considering the moderate luminescence and relatively stable emission of the $Cu_4(dppy)_4Cl_2$ NCs, we have evaluated its chemo sensing for ions detection. As shown in Fig. 5, a few common ions including Cu^{2+}, Fe^{3+}, K^+, Mg^{2+}, HCO_3^-, CO_3^{2-}, I^-, Cl^- (1.0 mmol/L for all) have been tested. It is found that the presence of Cl^- ions results in apparent increase of the emission intensity, which contrasts with all the other tested cationic and anionic ions. The chemo sensing toward Cl^- ions is likely associated with the distinct coordination interactions between Cl^- and the $Cu_4(dppy)_4Cl_2$ NCs.

In summary, we report here a comparative study of two phosphine-protected Cu NCs, $Cu_4(dppy)_4Cl_2$ and $Cu_{21}(dppy)_{10}$. The

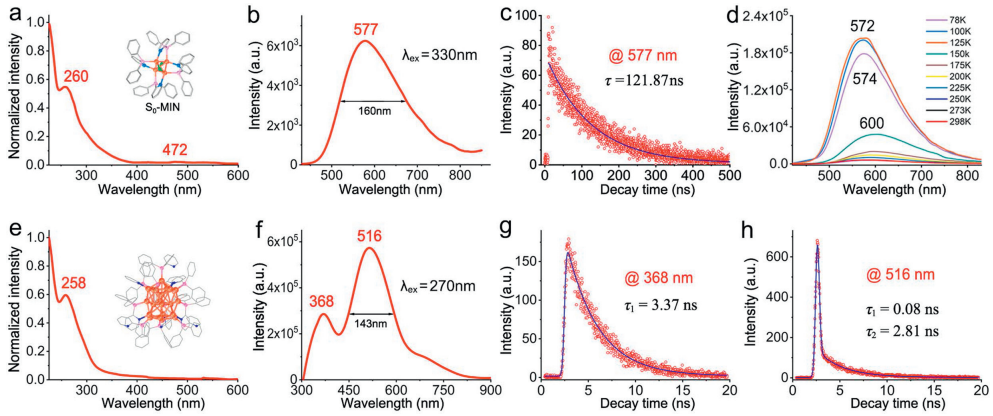

Fig. 3. (a, b) The absorption and photoluminescence spectra of the $Cu_4(dppy)_4Cl_2$ NCs in DCM. (c) Time-resolved emission decay at 298 K (λ_{ex} = 330 nm). (d) Temperature-dependant emission spectra at 78–298 K in DCM. (e, f) The absorption and photoluminescence spectra of the $Cu_{21}(dppy)_{10}$ NCs in DCM. (g, h) Time-resolved emission decay at 298 K (λ_{ex} = 270 nm).

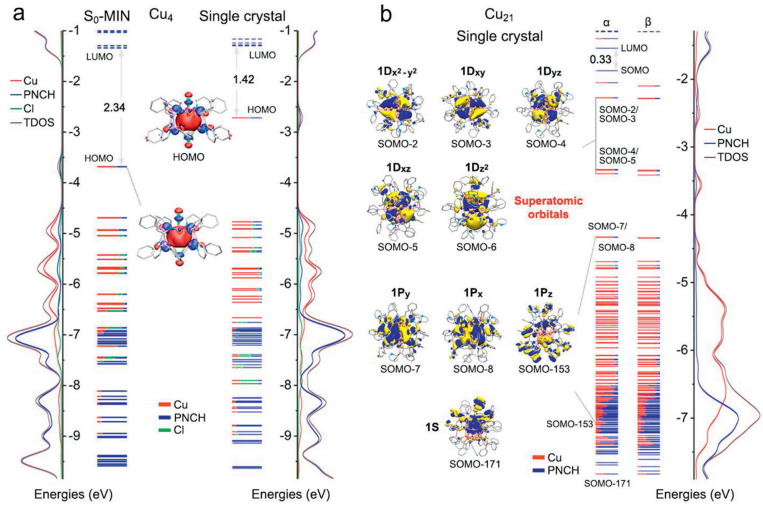

Fig. 4. Total and partial density of states (DOSs) and orbital energy levels of (a) $Cu_4(dppy)_4Cl_2$ based on the single-crystal structure and DFT-optimized S_0 minima, and (b) $Cu_{21}(dppy)_{10}$ based on the single crystal structure. Each orbital is drawn with colour labels to indicate the relative contributions of the atomic orbitals. The isosurface value of molecular orbitals is ±0.03 au H atoms are omitted for clarity.

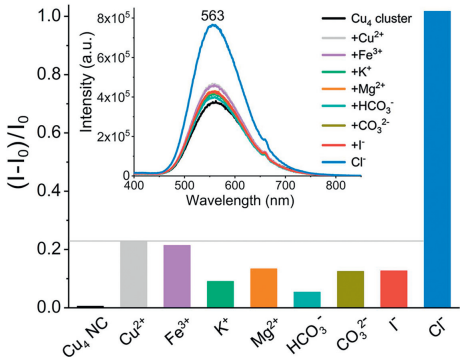

Fig. 5. The varied relative intensities of $Cu_4(dppy)_4Cl_2$ NCs (1 mg/mL, λ_{ex} = 330 nm) in the presence of typical testing ions (1.0 mmol/L). All the anions are sodium salts, while the cations are sulphates. The insets display the emission spectra of the $Cu_4(dppy)_4Cl_2$ nanoclusters in DMSO.

former has a tetrahedral Cu_4 core of which the six edges are fully protected by bridged chlorine and bidentate dppy ligands, while the latter has a Cu_{21} core pertaining to vivid superatomic states. The full passivation of the 2e-superatomic Cu_4 core accounts for its enhanced stability; in comparison, the stability of the larger cluster $Cu_{21}(dppy)_{10}$ is associated with its superatomic states of the Cu_{21} core, as well as well-organized ligand coordination and surface charge distribution. The ten dppy ligands form two types of coordination on the symetric Cu_{21} core, with four monodentate dppy ligands on the top one and bottom three Cu atoms through P-Cu bonds, while the other six dppy molecules as bidentate ligands to link 12 outside Cu atoms through both P-Cu bonds and N-Cu bonds. Interestingly, the $Cu_4(dppy)_4Cl_2$ NCs find an interesting yellow emission, while the $Cu_{21}(dppy)_{10}$ NCs exhibit dual emissions in the purple and green regions. We have conducted a chemo-sensing experiment by utilizing the red emission of $Cu_4(dppy)_4Cl_2$ NCs and find distinctive response to the chlorine anions.

Declaration of competing interest

The authors declare that they have no known competing financial interests or personal relationships that could have appeared to influence the work reported in this paper.

Acknowledgments

The authors thank Prof. Chunxi Zhang for friendly discussion. This work was financially supported by the National Natural Science Foundation of China (Nos. 22003072 and 21722308), the Min-

istry of Science and Technology of the People's Republic of China (No. 2020YFA0714602).

References

[1] M. Zhou, T. Higaki, G.X. Hu, et al., Science 364 (2019) 279–282.
[2] H. Zhen, X.Y. Dong, P. Luo, et al., Sci. Adv. 6 (2020) 1–8.
[3] G.T. Xu, L.L. Wu, X.Y. Chang, et al., Angew. Chem. Int. Ed. 58 (2019) 16297–16306.
[4] S.S. Zhang, L. Feng, R.D. Senanayake, et al., Chem. Sci. 9 (2018) 1251–1258.
[5] B. Yin, Z. Luo, Coord. Chem. Rev. 429 (2021) 213643.
[6] L. Ma, M. Melander, K. Laasonen, J. Akola, Phys. Chem. Chem. Phys. 17 (2015) 7067–7076.
[7] C. Guo, J. Irudayaraj, Anal. Chem. 83 (2011) 2883–2889.
[8] J. Wang, W. Xie, Y. Gao, et al., Sci. Bull. 63 (2018) 395–397.
[9] A.M. Pembere, C. Cui, R. Anumula, et al., Phys. Chem. Chem. Phys. 21 (2019) 17933–17938.
[10] R.S. Dhayal, W.E. van Zyl, C.W. Liu, Acc. Chem. Res. 49 (2016) 86–95.
[11] M.B. Gawande, A. Goswami, F.X. Felpin, et al., Chem. Rev. 116 (2016) 3722–3811.
[12] Y.R. Liu, S.C. Yiu, C.L. Ho, W.Y. Wong, Coord. Chem. Rev. 375 (2018) 514–557.
[13] S. Sharma, K.K. Chakrahari, J.Y. Saillard, C.W. Liu, Acc. Chem. Res. 51 (2018) 2475–2483.
[14] Y.L. Li, J. Wang, P. Luo, et al., Adv. Sci. 6 (2019) 1900833.
[15] Q. Du, B. Yin, S. Zhou, et al., Chin. Chem. Lett. 33 (2022) 995–1000.
[16] K. Shimada, A. Kobayashi, Y. Ono, et al., J. Phys. Chem. C 120 (2016) 16002–16011.
[17] T.-A.D. Nguyen, A.W. Cook, G. Wu, T.W. Hayton, Inorg. Chem. 56 (2017) 8390–8396.
[18] P. Roesch, J. Nitsch, M. Lutz, et al., Inorg. Chem. 53 (2014) 9855–9859.
[19] S. Tippireddy, R. Chetty, M.H. Naik, et al., J. Phys. Chem. C 122 (2018) 8735–8749.
[20] M.M. Zhang, X.Y. Dong, Z.Y. Wang, et al., Angew. Chem. Int. Ed. 59 (2020) 10052–10058.
[21] X.C. Shan, F.L. Jiang, D.Q. Yuan, et al., Chem. Sci. 4 (2013) 1484–1489.
[22] Q. Benito, X.F. Le Goff, S. Maron, et al., J. Am. Chem. Soc. 136 (2014) 11311–11320.
[23] X.L. Chen, R.M. Yu, X.Y. Wu, et al., Chem. Commun. 52 (2016) 6288–6291.
[24] Z. Luo, A.W. Castleman, Acc. Chem. Res. 47 (2014) 2931–2940.
[25] J. Li, M. Cui, H. Yang, et al., Chin. Chem. Lett. 33 (2022) 5147–5151.
[26] M.A. Tofanelli, C.J. Ackerson, J. Am. Chem. Soc. 134 (2012) 16937–16940.
[27] O. Lopez-Acevedo, H. Tsunoyama, T. Tsukuda, et al., J. Am. Chem. Soc. 132 (2010) 8210–8218.
[28] M. Zhu, C.M. Aikens, F.J. Hollander, et al., J. Am. Chem. Soc. 130 (2008) 5883–5885.
[29] M. Walter, J. Akola, O. Lopez-Acevedo, et al., Proc. Natl. Acad. Sci. U. S. A. 105 (2008) 9157–9162.
[30] K.K. Chakrahari, J.H. Liao, S. Kahlal, et al., Angew. Chem. Int. Ed. 55 (2016) 14704–14708.
[31] R.S. Dhayal, J.H. Liao, Y.C. Liu, et al., Angew. Chem. Int. Ed. 127 (2015) 3773–3777.
[32] L. Liao, S. Zhuang, C. Yao, et al., J. Am. Chem. Soc. 138 (2016) 10425–10428.
[33] J. Wei, R. Marchal, D. Astruc, et al., Angew. Chem. Int. Ed. 26 (2020) 5508–5514.
[34] W.J. Zhang, Z. Liu, K.P. Song, et al., Angew. Chem. Int. Ed. 60 (2021) 4231–4237.
[35] M. Walter, M. Moseler, R.L. Whetten, H. Häkkinen, Chem. Sci. 2 (2011) 1583–1587.
[36] P.D. Jadzinsky, G. Calero, C.J. Ackerson, et al., Science 318 (2007) 430–433.
[37] J.H. Jia, Q.M. Wang, J. Am. Chem. Soc. 131 (2009) 16634–16635.
[38] S. Jamali, Z. Mazloomi, S.M. Nabavizadeh, et al., Inorg. Chem. 49 (2010) 2721–2726.
[39] X.L. Pei, Y. Yang, Z. Lei, Q.M. Wang, J. Am. Chem. Soc. 135 (2013) 6435–6437.
[40] A. Del Zotto, E. Zangrando, Inorg. Chim. Acta 277 (1998) 111–117.
[41] J. Liu, C. Jacob, K.J. Sheridan, et al., Dalton Trans. 39 (2010) 7921–7935.
[42] Z. Lei, Z.J. Guan, X.L. Pei, et al., Chem. Eur. J. 22 (2016) 11156–11160.
[43] H. Wu, M. Yang, B. Huang, et al., Sci. China Chem. 65 (2022) 1594–1600.
[44] M.P. Bogaard, J. Peterson, A.D. Rae, Acta Cryst. B 37 (1981) 1357–1359.
[45] R.T. Boeré, A.W. Cordes, R.T. Oakley, R.W. Reed, J. Chem. Soc. Chem. Commun. 10 (1985) 655–656.
[46] T. Chivers, J.F. Richardson, N.R.M. Smith, Inorg. Chem. 24 (1985) 2453–2458.
[47] R.T. Boere, A.W. Cordes, S.L. Craig, et al., J. Am. Chem. Soc. 109 (1987) 868–874.
[48] M. Jansen, S. Strojek, Z. Naturforsch. B 50 (1995) 1171–1174.
[49] J. Taraba, Z. Zak, Inorg. Chem. 42 (2003) 3591–3594.
[50] R. Bruckner, H. Haller, S. Steinhauer, et al., Angew. Chem. Int. Ed. 54 (2015) 15579–15583.
[51] U. Pal Chaudhuri, L.R. Whiteaker, L. Yang, R.P. Houser, Dalton Trans. (2006) 1902–1908.
[52] L. Yang, D.R. Powell, R.P. Houser, Dalton Trans. (2007) 955–964.
[53] K. Chen, J. Shearer, V.J. Catalano, Inorg. Chem. 54 (2015) 6245–6256.
[54] H.H. Nie, Y.Z. Han, Z.C. Tang, et al., J. Clust. Sci. 29 (2018) 837–846.
[55] K. Freitag, H. Banh, C. Gemel, et al., Chem. Commun. 50 (2014) 8681–8684.
[56] C. Ganesamoorthy, J. Weßing, C. Kroll, et al., Angew. Chem. Int. Ed. 53 (2014) 7943–7947.
[57] A.W. Cook, Z.R. Jones, G. Wu, et al., J. Am. Chem. Soc. 140 (2018) 394–400.
[58] K.K. Chakrahari, R.P.B. Silalahi, T.H. Chiu, et al., Angew. Chem. Int. Ed. 131 (2019) 4997–5001.
[59] Z. Mao, J. Huang, C. Che, et al., J. Am. Chem. Soc. 127 (2005) 4562–4563.
[60] E.L. Bennett, P.J. Murphy, S. Imberti, S.F. Parker, Inorg. Chem. 53 (2014) 2963–2967.
[61] T.A. Nguyen, Z.R. Jones, B.R. Goldsmith, et al., J. Am. Chem. Soc. 137 (2015) 13319–13324.
[62] M.S. Bootharaju, R. Dey, L.E. Gevers, et al., J. Am. Chem. Soc. 138 (2016) 13770–13773.
[63] M. Olaru, E. Rychagova, S. Ketkov, et al., J. Am. Chem. Soc. 142 (2020) 373–381.
[64] L. Bergmann, G.J. Hedley, T. Baumann, et al., Sci. Adv. 2 (2016) e1500889.
[65] R.K. Koninti, S. Satpathi, P. Hazra, J. Phys. Chem. C 122 (2018) 5742–5752.
[66] T.Q. Yang, B. Peng, B.Q. Shan, et al., Nanomaterials 10 (2020) 261.
[67] B. Yin, Q. Du, L. Geng, et al., J. Phys. Chem. Lett. 11 (2020) 5807–5814.
[68] M. Schutz, C. Gemel, M. Muhr, et al., Chem. Sci. 12 (2021) 6588–6599.